European Journal of Pharmaceutics and Biopharmaceutics 80 (2012) 478–489

Contents lists available at SciVerse ScienceDirect

European Journal of Pharmaceutics and Biopharmaceutics

journal homepage: www.elsevier.com/locate/ejpb

Research paper

Treatment of lung cancer via telomerase inhibition: Self-assembled nanoplexes versus polymeric nanoparticles as vectors for 2′-O-Methyl-RNA

N. Nafee [a,f], M. Schneider [a,b,*], K. Friebel [b], M. Dong [c], U.F. Schaefer [a], T.E. Mürdter [c,d], C.-M. Lehr [a,e]

[a] Biopharmaceutics and Pharmaceutical Technology, Saarland University, Saarbrücken, Germany
[b] Pharmaceutical Nanotechnology, Saarland University, Saarbrücken, Germany
[c] Dr. Margarete Fischer-Bosch-Institute of Clinical Pharmacology, Stuttgart, Germany
[d] University of Tübingen, Stuttgart, Germany
[e] Helmholtz Institute for Pharmaceutical Research Saarland (HIPS), Helmholtz Centre for Infection Research (HZI), Saarbrücken, Germany
[f] Department of Pharmaceutics, Faculty of Pharmacy, Alexandria University, Alexandria, Egypt

ARTICLE INFO

Article history:
Received 10 September 2011
Accepted in revised form 28 November 2011
Available online 17 December 2011

Keywords:
Telomerase inhibitor
Nanoparticles
Lung cancer
Aerosolization
Air-interface culture
TRAP assay

ABSTRACT

Antisense oligonucleotide, 2′-O-Methyl-RNA (OMR), is known as potent telomerase inhibitor for the treatment of lung cancer but limited by poor intracellular uptake. Chitosan-coated polymeric nanoparticles were compared to chitosan solution as non-viral vectors for OMR. The study investigated the role of chitosan properties and concentration in improving the efficiency of the nanocarriers in terms of loading, viability, cellular uptake, and telomerase inhibition in human lung cancer cell lines. Certain concentration of chitosan on nanoparticle surface is necessary to significantly increase the cellular uptake. However, excessive chitosan negatively affected the transfection efficiency. Self-assembled nanoplexes with chitosan polymer are preferentially adsorbed to the cell membrane rather than being internalized. Thus, polymeric nanoparticles proved to be superior to cationic polymers as carrier for antisense oligonucleotides. Charge cannot be considered the principle factor behind improved transfection. Uptake studies carried out on air-interface cell cultures to mimic *in vivo* conditions supported the results on normal cultures showing enhanced uptake of nanoplexes over naked oligonucleotides. OMR nanoplexes reduced telomerase activity by ~50% in A549 cells concluding the potential of the system as a safe, non-invasive, and efficient treatment for lung carcinoma. These data are prerequisites for the ongoing studies on lung perfusion model and *in vivo* experiments.

1. Background

Lung cancer is one of the leading causes of cancer-related death worldwide [1]. Based on the characteristics of the disease and its response to treatment, it can be classified into two main types: non-small-cell lung cancer (NSCLC) and small-cell lung cancer (SCLC) accounting for ~85% and 15% of all lung cancer, respectively. Current cancer therapy in general remains as in the past 50 years; surgery followed by radiotherapy and chemotherapy [2,3]. The usefulness of cancer chemotherapy is restricted by the dose-limiting toxicity of cytotoxic anticancer drugs and the occurrence of side effects [4]. Indeed, safer, more potent, and site-specific alternatives are needed.

One of the best and most recent prospects for attaining versatile targeted therapeutics is the use of antisense oligonucleotides (ASOs) as therapeutic agents against cancer [5,6]. Instead of binding to proteins to modulate their function, ASOs target the unwanted proteins at the mRNA level, halting production. In the field of cancer treatment, promising approaches focus on such therapies that target specific proteins and pathways involved in the growth and proliferation of cancer cells. Much interest has recently been evoked by telomerase, a ribonucleoprotein that adds telomeric repeats to the end of the telomeres [7] and therefore prevents telomere shortening occurring during cell proliferation. Telomerase activity has been detected in 80% of NSCLC but not in non-cancerous lung tissue [8], therefore representing a promising target to reduce uncontrolled growth of cancer cells. Several classes of telomerase inhibitors targeting different sites of the

Abbreviations: NSCLC, non-small-cell lung cancer; SCLC, small-cell lung cancer; ASOs, antisense oligonucleotides; OMR, 2′-O-Methyl-RNA; FAM-OMR, fluoresceinamine-labeled 2′-O-Methyl-RNA; cNP, chitosan-modified nanoparticles; FA-NP, fluoresceinamine-labeled nanoparticles; NPx, nanoplexes; PLGA, poly(D,L-lactide-*co*-glycolide); PVA, polyvinyl alcohol; MTT, (3-(4,5-dimethylthiazol-2-yl)-2,5-diphenyltetrazolium bromide; LDH, lactate dehydrogenase; PBS, phosphate buffered saline; AIC, air-interface culture; TEER, transepithelial electrical resistance; RRCA, rhodamine-labeled ricinus communis agglutinin I; DAPI, 4′,6-diamidino-2-phenylindole dihydrochloride.

* Corresponding author. Pharmaceutical Nanotechnology, Saarland University, Campus A4 1, D-66123 Saarbrücken, Germany. Tel.: +49 681 302 2438; fax: +49 691 302 4677.
E-mail address: Marc.Schneider@mx.uni-saarland.de (M. Schneider).

0939-6411/$ - see front matter © 2011 Elsevier B.V. All rights reserved.
doi:10.1016/j.ejpb.2011.11.019

telomerase complex or the telomeres have been recently evaluated [9]. The second generation antisense oligonucleotide 2′-O-Methyl-RNA (OMR) with a phosphorothioate backbone is a potent and sequence-selective inhibitor of telomerase [10]. However, the application of these nucleotide-based drugs is limited by many problems, namely their premature degradation in the body and their poor cellular uptake [11,12]. Accordingly, successful delivery of OMR requires the proper choice of a suitable carrier system to target the site of action [13].

In this context, nanocarriers have gained great attention as promising gene delivery systems for both plasmid DNA and ASOs, giving promises to new generation of therapeutics in terms of diagnosis, treatment, and prevention. Among the nanocarriers, nanoparticles have shown broad application [14,15].

PLGA nanoparticles were extensively applied as efficient, biocompatible, and biodegradable delivery system [16–18]. However, we previously demonstrated that the negative charge of these particles limited their binding potential to negatively charged RNA and minimized their interaction with the cell membrane. Surface modification of these particles with a cationic polymer, chitosan, improved their internalization by cancerous cells [19]. Furthermore, chitosan alone was extensively applied to form self-assembling complexes with anionic plasmids owing to its relative safety, permeability enhancing properties, and efficiency as gene carrier [20,21]. Yet it was not clear whether the self-assembled chitosan/OMR nanoplexes would have better or at least the same potential as nanoplexes formed of chitosan-modified PLGA nanoparticles (cNP) and the antisense oligonucleotides. Therefore, our aims were; first, to weigh up self-assembled versus surface-modified polymeric nanocarriers as vectors for antisense oligonucleotides. Second, to obtain deeper insight on the influence of the surface charge and different chitosan properties on binding, uptake, and transfection efficiency for better understanding and to point out the key parameters affecting the transfection process.

In this context, the intracellular uptake of fluorescently labeled nanoparticles containing increasing concentrations of chitosan as well as their corresponding nanoplexes with fluorescently labeled oligonucleotides in different human cancer cell lines were investigated. Furthermore, simple self-assembled nanoplexes of OMR with different types of chitosan were also studied in parallel. To mimic the *in vivo* conditions in the pulmonary tract, the ordinary cell culture was replaced by air-interface culture (AIC). This gives a better and more realistic idea about the deposition and uptake of nanoparticles on the cell monolayer [22].

As our target is the inhibition of telomerase not just the internalization of the nanoplexes, but the effect of OMR as a telomerase inhibitor was evaluated based on the reduction of telomerase activity as a function of chitosan content.

2. Materials and methods

2.1. Materials

Poly(D,L-lactide-*co*-glycolide) 70:30 (Polysciences Europe GmbH, Eppelheim, Germany), polyvinyl alcohol (PVA) Mowiol® 4-88 (Kuraray Specialities Europe GmbH, Frankfurt, Germany), different types of ultrapure chitosan: the chloride salts; Protasan® UP CL113 and Protasan® UP CL213, and the glutamate salts; Protasan® UP CG113 and Protasan® UP CG213 with different properties (see Table 1) (FMC BioPolymer AS, Oslo, Norway), 5-Fluoresceinamine (FA) and 1-ethyl-3-(3-dimethylaminopropyl)-carbodiimide hydrochloride (DMAP) (Sigma Chemical Co., St. Louis, MO, USA), ethyl acetate (Fluka Chemie GmbH, Buchs, Switzerland) were used as obtained. The antisense oligonucleotide 2′-O-Methyl-RNA (OMR) with a phosphorothioate (ps) backbone (5′-2′-O-methyl [C(ps)A(ps)GUUAGGGUU(ps)A(ps)G]-3′), the carboxyfluorescein-amine-labeled derivative 5′-FAM-OMR and the mismatch (5′-2′-O-methyl [C(ps)A(ps)GUUAGAAUU(ps)A(ps)G]-3′) were obtained from Biomers.net GmbH (Ulm, Germany).

2.2. Methods

2.2.1. Fluorescent labeling of PLGA

Fluoresceinamine-bound PLGA (FA-PLGA) was prepared based upon the method described by Horisawa et al. [23] and Weiss et al. [24]. Briefly, appropriate amounts of PLGA and FA were dissolved entirely in acetonitrile and stirred overnight with DMAP at room temperature (20 °C). The resulting FA-PLGA was precipitated by the addition of purified water and separated by centrifugation at 1000*g* (Universal 30RF, Hettich Centrifuges, Tuttlingen, Germany). The polymer was rinsed from excessive reagents (repeated dissolvation in acetone and precipitation with ethanol) and then lyophilized (Alpha 2-4 LSC, Martin Christ Gefriertrocknungsanlagen GmbH, Osterode, Germany).

2.2.2. Preparation and characterization of nanoparticles

PLGA nanoparticles (NP-0) and chitosan-modified PLGA nanoparticles containing increasing concentration of chitosan 0.3–1.2%w/v (denoted by NP-3–NP-12, respectively) were prepared by the emulsion–diffusion–evaporation technique as previously described [19]. Briefly, PLGA in ethyl acetate was added dropwise to an equal volume of the aqueous phase (PVA solution with or without chitosan chloride, Protasan® UP CL113) under stirring (1000 rpm, 1 h). The emulsion was homogenized (Ultra-Turrax T25; Janke & Kunkel GmbH & Co-KG, Germany) at 13,500 rpm, 10 min. MilliQ water was added dropwise under gentle stirring to allow solvent diffusion and nanoparticle formation. Stirring was continued overnight at room temperature (20 °C) to evaporate the organic solvent. Fluorescently labeled nanoparticles of the same formulations mentioned above were prepared using FA-PLGA and denoted by FA-NP-0 to FA-NP-12 (Table 2). Nanoparticles were purified from excess unbound polymers based on centrifugal ultrafiltration using Centrisart I, Sartorius AG, Goettingen, Germany (on small scale), or size exclusion chromatography (on large scale). The amount of residual polymers (PVA and chitosan) was quantified using colorimetric assays. PVA content was quantified based on the formation of a greenish colored complex between two adjacent hydroxyl groups of PVA and iodine molecule in the presence of boric acid [25]. Regarding chitosan, the presence of residual unbound chitosan in the supernatant was verified by means of a colorimetric assay based on the ionic interaction between the protonated amino groups of chitosan and sulfonic acid groups on the ionic dye, Cibacron Brilliant Red [26]. Detailed description of the assays is provided in Supplementary materials.

Nanoparticles were freeze-dried (Alpha 2-4 LSC, Martin Christ Gefriertrocknungsanlagen GmbH, Osterode, Germany). The physicochemical properties (size and ζ-potential) of plain and fluorescently labeled nanoparticles were measured using Malvern Zetasizer Nano (Malvern Instruments, Malvern, UK). The colloidal stability of the particles after purification and freeze-drying was verified. Concentrations of nanoparticles were determined gravimetrically after lyophilization.

2.2.3. Loading of nanoparticles with oligonucleotides; formation and characterization of nanoplexes

Nanoparticles NP-0 to NP-12 were loaded with 2′-O-Methyl-RNA at different weight ratios and vortexed for 30 s followed by 10 min incubation on an orbital shaker at room temperature (20 °C). Self-assembled nanoplexes were prepared by simple mixing of OMR with chitosan salt solution (Protasan® UP CL113, Protasan® UP CL213, Protasan® UP CG113 and Protasan® UP CG213) in a

Table 1
Properties of different types of chitosan.

Type of chitosan	Formula code	Chitosan properties	
		Molecular weight[a] (kDa)	Viscosity[b] (mPa s)
Protasan® UP CL113	CL113	<150	<20
Protasan® UP CL213	CL213	150–400	20–200
Protasan® UP CG113	CG113	<200	<20
Protasan® UP CG213	CG213	200–600	20–200

[a] Approximate molecular weight (weight average molecular weight).
[b] Standard viscosity ranges (1% solution, 20 °C).

Table 2
Colloidal characteristics of PLGA nanoparticles modified with different concentrations of chitosan.

Chitosan content (%w/v)	Plain nanoparticles				Fluorescently labeled nanoparticles			
	Code	Particle size (nm)	PI	ζ-potential (mV)	Code	Particle size (nm)	PI	ζ-potential (mV)
0	NP-0	145.7 ± 1.6	0.05 ± 0.02	−19.2 ± 0.1	FA-NP-0	156.3 ± 4.9	0.037 ± 0.015	3.2 ± 0.3
0.3	NP-3	203.1 ± 1.7	0.16 ± 0.01	30.5 ± 1.24	FA-NP-3	177.7 ± 3.1	0.07 ± 0.021	22.3 ± 2.7
0.6	NP-6	228.1 ± 3.3	0.18 ± 0.02	39.2 ± 2.1	FA-NP-6	174.9 ± 2.1	0.113 ± 0.014	33.7 ± 0.6
0.9	NP-9	250.8 ± 0.9	0.22 ± 0.01	52.6 ± 0.76	FA-NP-9	198.2 ± 2.0	0.127 ± 0.018	39.1 ± 0.7
1.2	NP-12	250.3 ± 3.2	0.20 ± 0.01	55.9 ± 0.14	FA-NP-12	201.7 ± 3.7	0.148 ± 0.012	46.2 ± 4.0

concentration equivalent to that used during nanoparticle preparation.

The colloidal characteristics (size and ζ-potential) of NP/OMR nanoplexes were determined using Malvern Zetasizer Nano (Malvern Instruments, Malvern, UK). Measurements were performed in triplicates.

2.2.4. Cell cultures

2.2.4.1. A549 cells. (CCL-185; ATCC, Manassas, VA, USA) were cultivated in RPMI with L-glutamine (PAA Laboratories GmbH, Pasching, Austria) supplemented with 10% fetal calf serum (FCS).

2.2.4.2. Calu-3 cells. (HTB-55; ATCC, Manassas, VA, USA) were cultivated in Minimum Essential Medium (MEM) with Earl's Salts and L-glutamine (PAA Laboratories GmbH, Pasching, Austria) supplemented with 10% FCS, 1% non-essential amino acid (NEAA) solution, and 1 mM sodium pyruvate (all from Sigma–Aldrich Chemie GmbH, Steinheim, Germany).

2.2.4.3. Air-interface cultures. (AIC) were seeded onto the membrane culture insert (Costar Transwell 3460, pore size 0.4 μm, Corning, Cambridge, MA, USA). After reaching a constant transepithelial electrical resistance (TEER) value, the culture medium was removed from the apical side and the cell monolayer continued to grow on AIC for 5 days.

2.2.5. Cytotoxicity assays

A549 and Calu-3 cells were incubated with nanoparticles with increasing chitosan concentrations (NP-0 → NP-12) at a concentration of 0.88 mg/ml. In addition, NP-3 was incubated with A549 cells in different concentrations (0.1–2.5 mg/ml) in culture medium for 6 h. The supernatants were transferred to 96-well plates for lactate dehydrogenase (LDH) assay (investigation of cell membrane integrity) whereas cells in the original plates were washed with phosphate buffered saline (PBS) and allowed to grow for 24 h in culture medium for MTT ((3-(4,5-dimethylthiazol-2-yl)-2,5-diphenyltetrazolium bromide) assay (to determine cell viability). A mean value of four replicates was determined.

2.2.6. Cell association and intracellular uptake studies

2.2.6.1. Flow cytometry. A549 cells (100,000 cell/ml) and Calu-3 cells (300,000 cell/ml) were seeded in multiwell plates 24 and 72 h, respectively, prior to the experiment. Non-treated cells, cells treated with fluorescently labeled oligonucleotides in addition to cells treated with nanoparticles only were used as control. Samples investigated ($n = 4$) include fluorescently labeled nanoparticles with increasing chitosan content (FA-NP-0 to FA-NP-12), nanoplexes of FAM-OMR with different nanoparticle formulations in the ratio 1:50, and self-assembled nanoplexes with chitosan solution of different properties (CL113, CL213, CG113, CG213). Samples to be investigated were mixed with the culture medium and incubated with the cells for 6 h. Nanoplexes were then replaced with fresh medium after several washing steps and the cells were incubated until the next day where the green fluorescence of the labeled oligonucleotides was measured at 488 nm. Analysis by flow cytometry was performed the next day with a FACSCalibur flow cytometer from Becton Dickinson (BD) Biosciences (Heidelberg, Germany) using the software CellQuest™ Pro Version 4.02 (BD Biosciences). Cell association was evaluated after gating and definition of a fluorescence threshold with non-treated cells.

2.2.6.2. Confocal Laser Scanning Microscopy (CLSM). A549 and Calu-3 cells were seeded on LabTec chamber slides (Nunc GmbH, Wiesbaden, Germany) at a density of 12,500 and 100,000 cells/ml, respectively. Cells were incubated with FA-NPs or nanoplexes with FAM-OMR (4 μm) in the weight ratio OMR:NP (1:50) ($n = 3$). After 6 h of incubation, the medium was replaced by normal cell culture medium. The cells were stained after 24 h, and then examined by CLSM.

Cell membranes were stained with the red fluorescent Rhodamine-labeled ricinus communis agglutinin I (RRCA; $\lambda_{ex} = 552$ nm, $\lambda_{em} = 577$ nm; Vector Laboratories Peterborough, UK), then fixed with 4% paraformaldehyde in PBS. The nuclei were then stained with 4′,6-diamidino-2-phenylindole dihydrochloride (DAPI, $\lambda_{ex} = 374$ nm, $\lambda_{em} = 461$ nm; Fluka Chemie GmbH, Buchs, Switzerland).

Fluorescence imaging was performed using a Zeiss 510 LSM META NLO confocal laser scanning microscope (Jena, Germany). The setup made use of a 100× objective and of an argon ion laser line at $\lambda = 488$ nm to excite the oligonucleotides, a HeNe-laser with $\lambda = 542$ nm to excite RRCA, and a pulsed Ti:Sapphire laser operating at $\lambda = 730$ nm (~150 fs pulses, 80 MHz repetition rate) to excite DAPI based on the adsorption of two or more photons. The green fluorescent nanoparticles/nanoplexes were located with respect to the red-stained cell membrane and the blue-stained cores.

The uptake efficiency was determined by counting the number of transfected cells relative to the total number of cells in different areas of the sample (~10 areas/sample).

2.2.7. Nebulization and uptake on air-interface cultures

A hydraulic liquid microsprayer Penn Century® (Model IA-1C, Penn Century Inc., Philadelphia, USA) was used for nebulization of nanoparticles on AIC. The colloidal characteristics of the samples were verified after nebulization. Nanoplexes of FAM-OMR with NP-3 in the ratio 1:50 were sprayed over the surface of AI-cultured A549 cells using the Penn Century®. After 6 h incubation, cell surfaces were washed, fixed, and stained as mentioned above. The green fluorescence of the FAM-labeled oligonucleotides was examined by CLSM. In addition, the effect of nebulization on cell viability and membrane integrity was checked.

2.2.8. Reduction in telomerase activity (TRAP assay)

The activity of OMR (either alone or as nanoplexes) following the cellular uptake was investigated by measuring the telomerase activity by real-time PCR-based Telomeric Repeat Amplification Protocol (TRAP assay). A549 cells were incubated with OMR nanoplexes formed with nanoparticles of increasing chitosan content (NP-0–NP-12) in the ratio 1:50 for 6 h, then replaced by cell culture medium. Cells incubated with the corresponding plain nanoparticles were also assessed for comparison. In addition, nanoplexes formed with a mismatch instead of the OMR were used to check the specificity of the measurements. 72 h following incubation, A549 cells (1×10^6) were collected and lysed in 200 μl ice-cold CHAPS lysis buffer (10 mM Tris–HCl (pH 7.5), 1 mM $MgCl_2$, 1 mM EDTA, 0.1 mM Benzamidine, 5 mM β-mercaptoethanol, 0.5% CHAPS (3-[(3-cholamidopropyl)dimethyl-ammonio]-1-propanesulfonate), 10% glycerol) for 30 min on ice. Lysates were centrifuged at 12,000*g* for 20 min at 4 °C and the supernatants were snap-frozen and stored at −80 °C.

Telomerase activity was measured using an optimized real-time quantitative PCR-based telomeric repeat amplification protocol (Q-TRAP) assay [27]. Briefly, Q-TRAP reaction was performed with 50 ng telomerase primer TS, 50 ng anchored return primer ACX, SYBR Green PCR Master Mix (QuantiTect®, QIAGEN, Hilden, Germany), and 2 μl cell extract containing 0.1 μg protein in 384-well clear optical reaction plates (MicroAmp®, Applied Biosystems, USA). The 7900HT Fast Real-Time PCR System (Applied Biosystems, USA) was used. Samples were first incubated for 30 min at 30 °C for telomerase mediated extension reaction (if present), then 95 °C for 1 min followed by 40 cycles of 94 °C for 15 s, 60 °C for 60 s. The threshold cycle value (*Ct*) of each sample was determined from amplification log plots (the change in fluorescent signal was plotted against cycle number). Calibration curves were generated from serial dilutions of telomerase-positive human lung cancer cell line A549 cell extracts with 1.0, 0.2, 0.04, 0.008, and 0.0016 μg of protein, respectively. Negative control samples were created by heat inactivation at 85 °C for 10 min. Telomerase activity of each sample was expressed as relative telomerase activity (RTA) to reference A549 cells (telomerase activity of 1 μg protein of A549 cell extracts was defined as 1). The sequences of the primers are as follows: TS primer 5′-AATCCGTCGAGCAGAGTT-3′ and ACX primer 5′-GCGCGGCTTACCCTTACCCTTACCCTAACC-3′. All measurements were performed in quadruplicates.

2.2.9. Statistical analysis

Data are expressed as mean ± standard deviation and analyzed by *t*-test, one/two-way ANOVA (SigmaStat 3.0, SPSS Inc. Chicago, IL, USA). Values of $p \leqslant 0.05$ were indicative of significant differences.

3. Results

3.1. Characterization of nanoparticles

Plain and fluorescently labeled nanoparticles containing increasing concentrations of chitosan, Protasan® UP CL113, were characterized in terms of particle size, polydispersity index (PI), and ζ-potential. The colloidal characteristics of these particles are summarized in Table 2. Previous study indicated that different types of chitosan had insignificant changes in nanoparticle size and charge [19].

Increasing the amount of chitosan resulted in a gradual increase in nanoparticle size from 145.7 to 250.3 nm and ζ-potential from −19.2 to +55.9 mV indicating efficient surface localization of the positively charged polymer on the nanoparticle surface. The same tendency was observed for nanoparticles prepared using FAM-labeled PLGA. Fig. 1A illustrates the spherical shape and smooth surface of the nanoparticles.

Colorimetric assays used to quantify the amount of residual polymers indicated that ~33% of PVA remained unbound in the supernatant whereas >90% of the chitosan was bound to the nanoparticle surface. This finding is supported by our previous study [19] that investigated the effect of increasing chitosan concentration from 0.15 to 1.5 mg/ml on the physicochemical properties of nanoparticles. ζ-Potential values fitted revealed incomplete surface saturation with chitosan within the concentration range used in the actual study.

Particles retained their colloidal characteristics (size and ζ-potential) after purification and freeze-drying.

3.2. Formation and characterization of nanoplexes

Complexes of different nanoparticle formulations (NP-0–NP-12) with OMR at various OMR:NP weight ratios (ranging from 1:100 to 1:1) were termed nanoplexes (NPX). As demonstrated in Fig. 1B, the size of the nanoplexes differ by ~50 nm from the size of the plain nanoparticles with the exception of nanoplexes formed at 1:10 and sometimes 1:200 OMR:NP ratio where a distinct increase in size and PI of chitosan-modified PLGA NPs was observed revealing partial agglomeration, Fig. 1B and C. This was not noticed in case of OMR nanoplexes with PLGA nanoparticles, suggesting no complexation [28].

In addition, increasing OMR concentration resulted in gradual reduction of ζ-potential, Fig. 1D, indicating surface binding or loading of the negatively charged OMR on particle surface. For weight ratios of OMR:NP 1:10 and 1:1, the surface charge is changing from positive to negative values (isoelectric point). Equal weight concentration of OMR and NPs lead to complete saturation. A net negative ζ-potential of ~−20 mV was recorded for all NPX.

3.3. Cytotoxicity assays

A549 and Calu-3 cells showed a survival rate ranging from 70% to 100% after incubation with 0.88 mg/ml nanoparticles with increasing chitosan content (NP-0 → NP-12) as estimated by MTT assay, Fig. 2A. Chitosan concentration had statistically insignificant effect on cell viability of Calu-3 cells (*One-way ANOVA*, $p < 0.05$). For A549 cells, a certain effect was observed reducing the metabolic activity of the cells. Further investigations on NP-3 concentration (0.1–2.5 mg/ml) showed 80–90% viability of A549 and negligible effect on the membrane integrity (LDH assay) Fig. 2B, (*One-way ANOVA*, $p < 0.05$).

3.4. Flow cytometry

Flow cytometry was used to measure the increase in fluorescence of A549 cells after incubation with different fluorescent

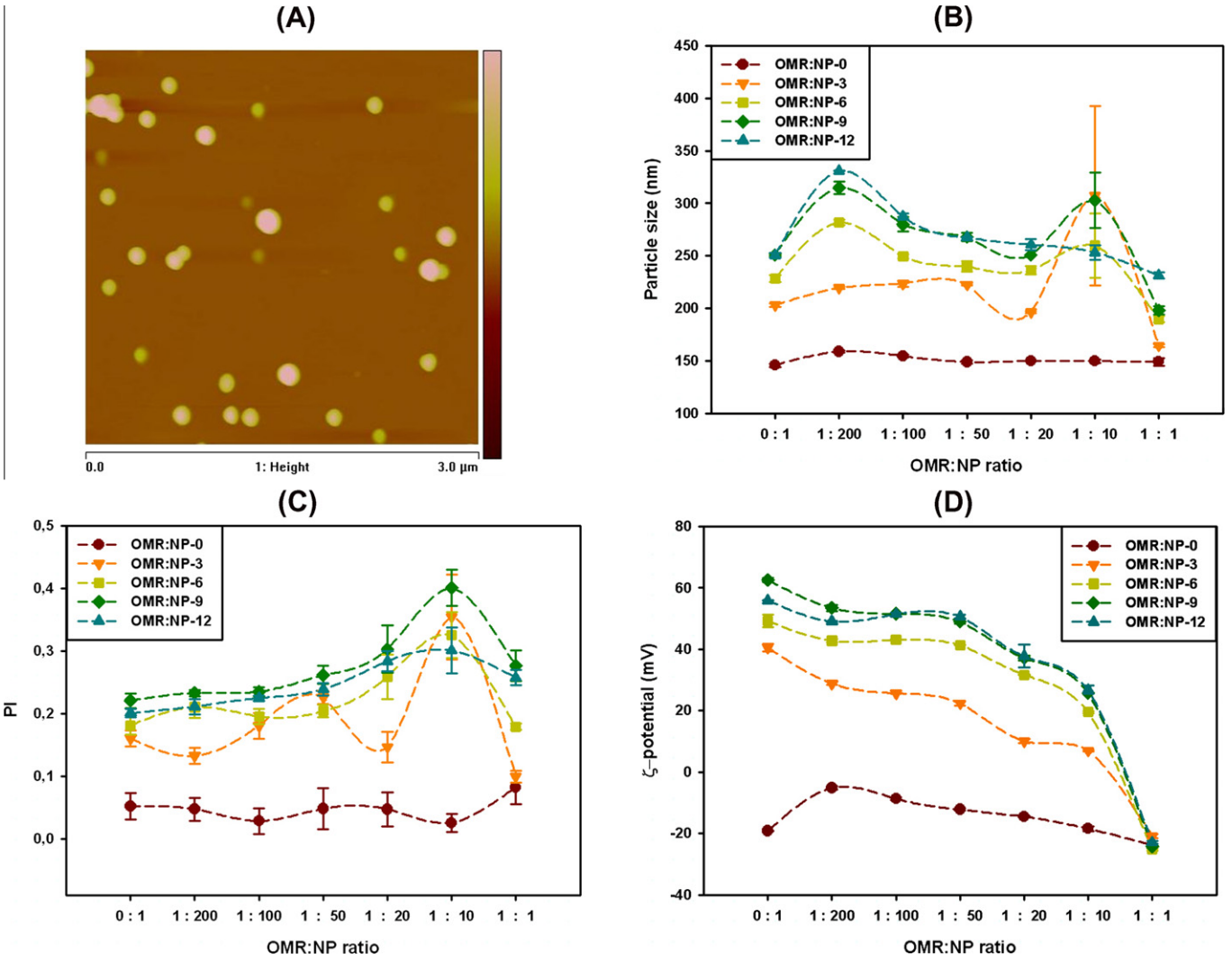

Fig. 1. (A) AFM image under ambient conditions in tapping mode of plain chitosan-coated nanoparticles, Properties of nanoplexes of OMR with PLGA nanoparticles coated with increasing chitosan concentrations: (B) size, (C) polydispersity index, and (D) ζ-potential at different OMR: NP ratio.

nanoparticles. Results were presented as % increase in fluorescence intensity compared to control cells, Fig. 3A. A significant increase in fluorescence was observed in case of FA-NP-3 compared to FA-NP-0 (*One-way ANOVA*, $p < 0.05$). Further increase in the chitosan content was not accompanied by a corresponding increase in fluorescence, on the contrary, the peaks were gradually shifted backwards to get very weak fluorescence with FA-NP-12 comparable to FA-NP-0.

Binding/uptake of self-assembled nanoplexes of OMR with chitosan of different properties (CL113–CG213) was shown by 60% increase in fluorescence intensity of A549 cells, Fig. 3B, but no significant effect of chitosan molecular weight and viscosity was noticed (*One-way ANOVA*, $p < 0.05$). Fluorescence signal was highly dependent on both chitosan content and cell type; fluorescently labeled oligonucleotides and their complexes with PLGA NPs (OMR/NP-0) show limited interaction with both A549 and Calu-3 cells, Fig. 3C. Although the presence of chitosan enhanced the adsorption/uptake with A549 cells, nanoplexes with NP-3 (OMR:NP-3 in the ratio 1:50) and chitosan solution (OMR/CL113) show <5% fluorescence in case of Calu-3 cells compared to >60% in case of A549 cells (*Significant difference*, *Two-way ANOVA*, $p < 0.05$).

3.5. Confocal Laser Scanning Microscopy (CLSM)

Fig. 4 demonstrates the uptake of labeled nanoparticles in A549 cells using CLSM, where the membranes were stained with RRCA – an adsorbing red dye bound to a lectin – and the nuclei stained in blue with DAPI. Localization of FA-NPs was detected by making sections in *z*-direction of the cells. As a result, *xz*- and *yz*-cross sections from 3D stacks allowed determining the location of the particles relative to the red-stained apical cell surface and the blue-stained nuclei. A significant green fluorescence was observed in A549 cells incubated with chitosan-modified nanoparticles, FA-NP-3, FA-NP-6, and FA-NP-9, compared to the control (non-treated cells) and those incubated with FA-NP-0 (Fig. 4A–E). Notably, FA-NP-12 containing highest content of chitosan were very poorly internalized, Fig. 4F, instead, some agglomerates were observed on the cell surface. The cross sections show the green fluorescence as point-shaped spots, mainly in the cytoplasm indicating their possible entrapment in intracellular vesicles.

Nanoplexes of FAM-OMR with non-labeled NP formulations (NP-0–NP-12) were prepared with OMR:NP weight ratio 1:50 and added to the cells for 6 h. Fig. 5 represents the uptake of the nanoplexes 24 h after incubation with A549 cells. OMR/NP-0 nano-

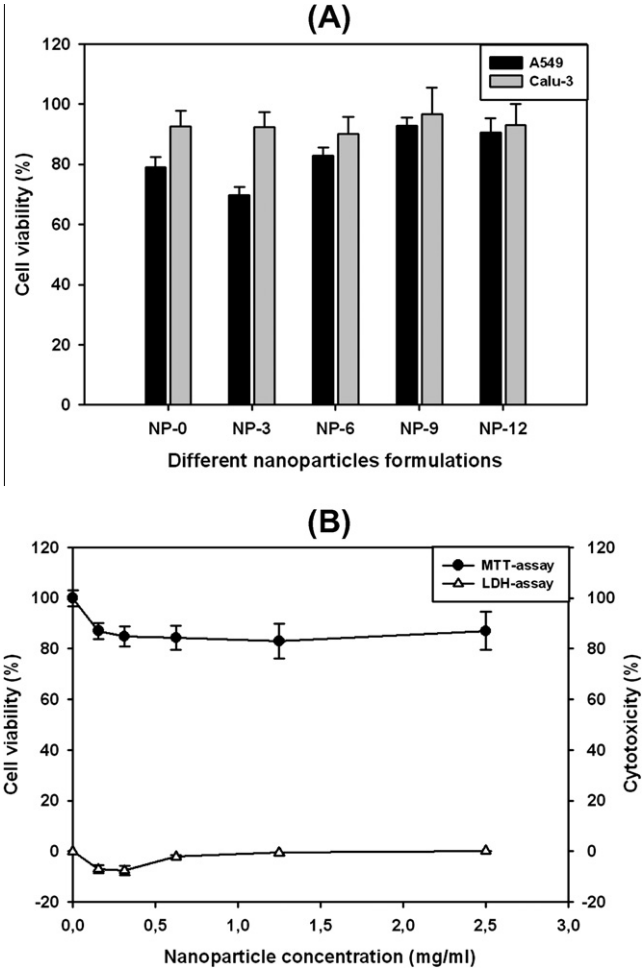

Fig. 2. (A) Viability of A549 and Calu-3 cells measured by MTT assay after 6 h incubation with different nanoparticle formulations (NP-0 → NP-12) at a concentration of 0.88 mg/ml, (B) viability (MTT assay, black circles) and membrane integrity (LDH assay, white triangles) of A549 cells after 6 h incubation with different concentrations of NP-3 (0.1–2.5 mg/ml).

plexes showed small fluorescence signal from inside the cells, Fig. 5B, whereas OMR/NP-3 were efficiently internalized as noticed by the significant amount of fluorescent spots in the cells, Fig. 5C. In correlation with uptake results of FA-NPs, the uptake of OMR nanoplexes with NP-6–NP-12 was lower compared to OMR/NP-3 nanoplexes indicating that increasing chitosan content in the nanoparticles above certain limit is not correlated with a consequent improvement in cellular uptake. In addition to green spots in the cytoplasm, agglomerates of OMR/NP-12 nanoplexes on the cell surface can be observed, which might explain their poor internalization as in case of FA-NP-12, Fig. 5F.

Incubation of FA-NPs with Calu-3 cells resulted in a relatively weak intracellular uptake independent of chitosan content on the NP surface. This was illustrated by the CLSM images provided in Supplementary materials, Fig. S1. Therefore, further uptake studies using OMR nanoplexes in Calu-3 cells were not performed.

CLSM images of self-assembled nanoplexes of OMR with chitosan of different properties in A549 cells showed significant amount of fluorescent nanoplexes agglomerated as patches on the outer surface of the cell membrane. This is indicated by the overlap of the green-labeled nanoplexes and red fluorescence of the membrane observed as yellowish areas, Fig. 6A–D, suggesting strong interaction with the cell membrane. Uptake was also observed to a smaller extend. No significant difference in uptake as a function

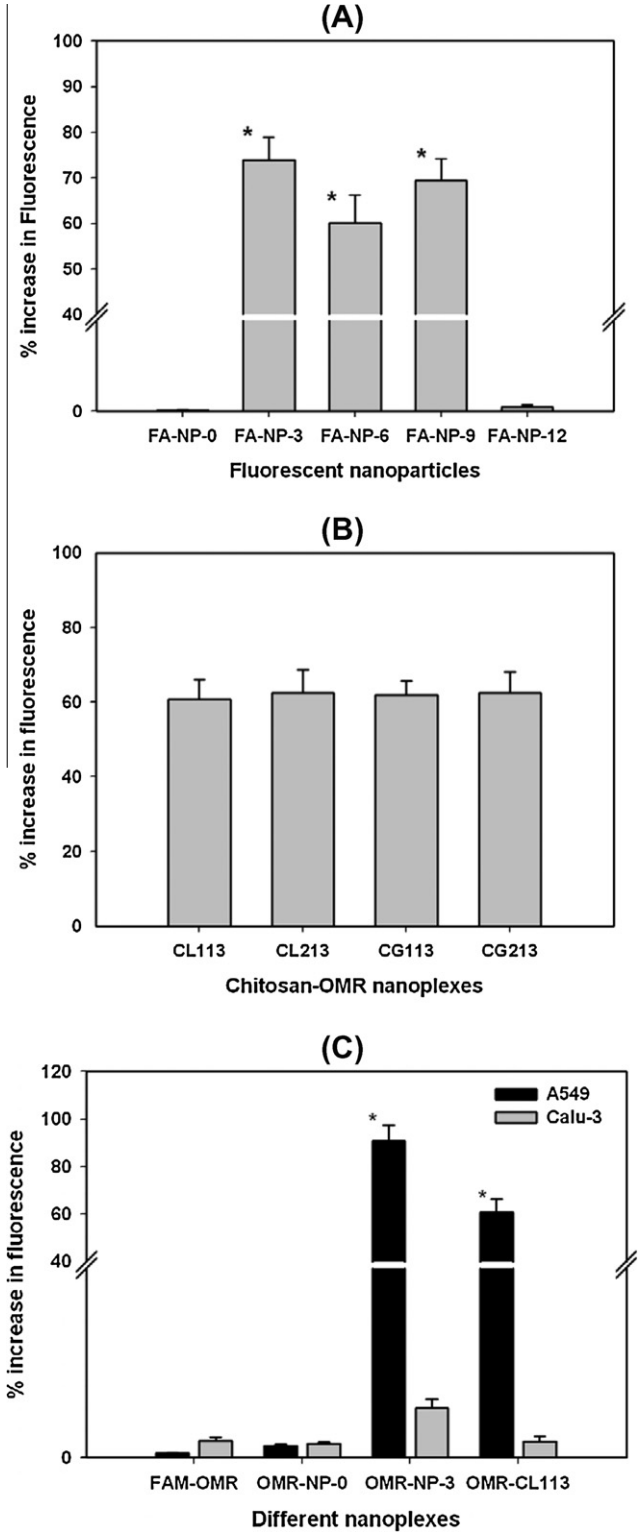

Fig. 3. Flow cytometry: percentage increase in green fluorescence of A549 cells after 6 h incubation with: (A) fluorescently labeled nanoparticles (FA-NP-0 → FA-NP-12) (*significant difference between either NP-3, NP-6, or NP-9 when compared to NP-0 and NP-12, one-way ANOVA, $p < 0.05$), (B) self-assembled OMR nanoplexes with increasing concentrations of chitosan (insignificant difference in fluorescence after incubation of A549 cells with OMR nanoplexes with different types of chitosan, one-way ANOVA, $p < 0.05$), (C) Flow cytometry of A549 and Calu-3 cells after incubation with different types of nanoplexes (*significant difference in fluorescence between A549 cells versus Calu-3 cells when both were incubated with OMR-NP-3, similar significance in case of OMR-CL113 nanoplexes, *OMR-NP-3 and OMR-CL113 nanoplexes show significantly high fluorescence compared to OMR alone and OMR-NP-0 nanoplexes in A549 cells, two-way ANOVA, $p < 0.05$).

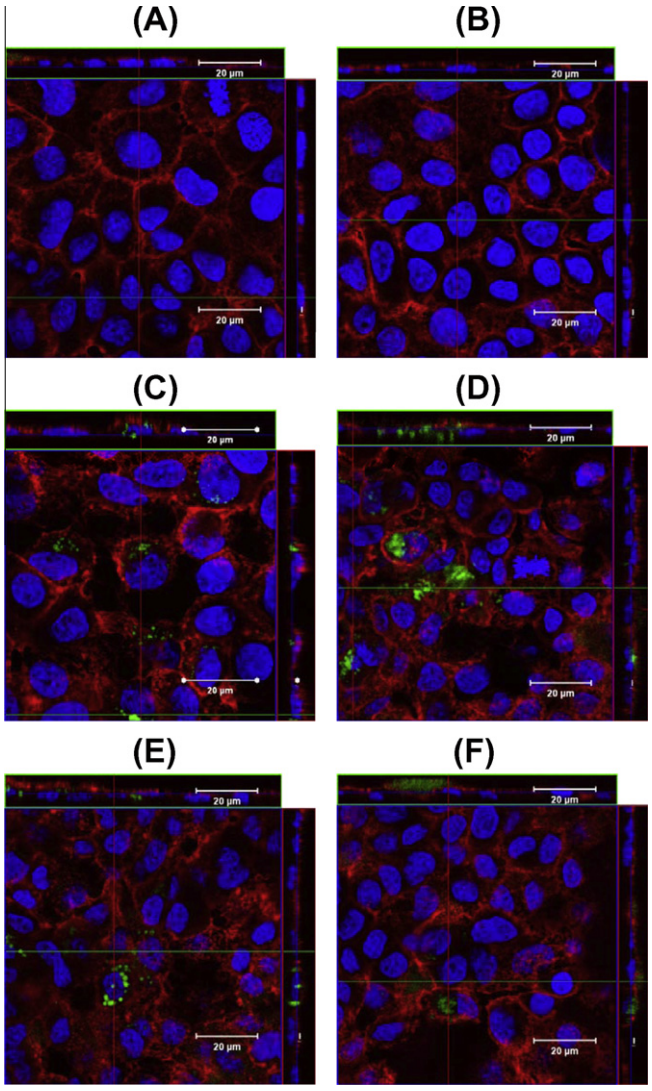

Fig. 4. CLSM images showing the uptake of different fluorescently labeled nanoparticles in A549 cells after 6 h incubation: (A) control cells, (B) FA-NP-0, (C) FA-NP-3, (D) FA-NP-6, (E) FA-NP-9, (F) FA-NP-12. Green fluorescence: FA-nanoparticles, red fluorescence: cell membrane counterstained with RRCA, and blue fluorescence: nuclei stained with DAPI. CLSM images 24 h after incubation with cells, green and red lines indicate the position of *xz*- and *yz*-cross sections through image stacks. Remarkable green fluorescence in C, D, and E observed mainly in the cytoplasm, higher chitosan content in FA-NP-12 caused nanoparticle aggregation on the cell surface and limited uptake.

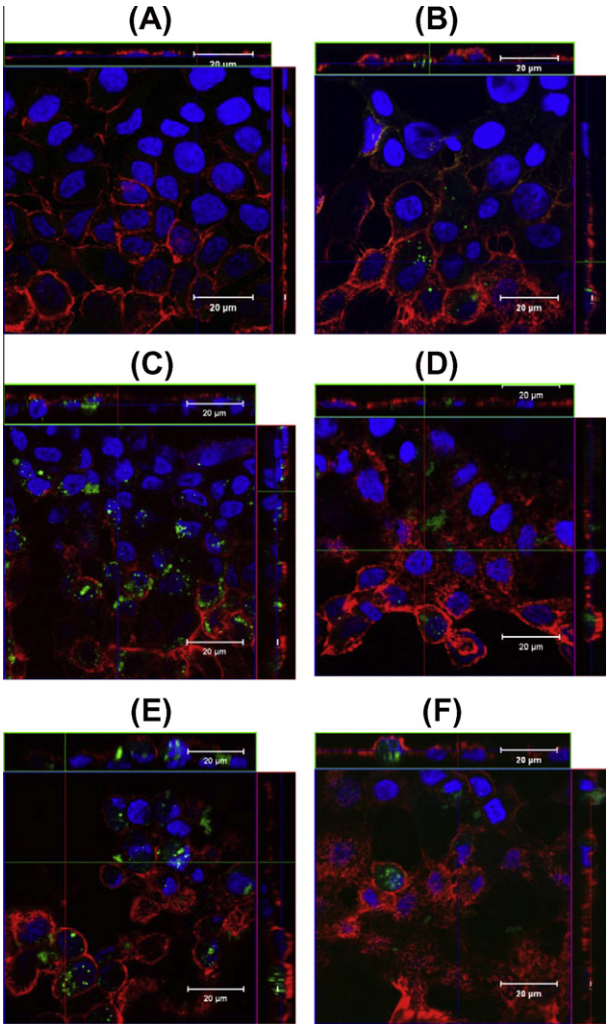

Fig. 5. CLSM images showing the uptake of OMR nanoplexes with different nanoparticles in the ratio OMR:NP 1:50 after 6 h incubation with A549 cells: (A) control cells, (B) OMR/NP-0, (C) OMR/NP-3, (D) OMR/NP-6, (E) OMR/NP-9, (F) OMR/NP-12. Green fluorescence: FAM-OMR, red fluorescence: cell membrane counterstained with RRCA, and blue fluorescence: nuclei stained with DAPI. CLSM images 24 h after incubation with cells, green and red lines indicate the position of *xz*- and *yz*-cross sections through image stacks. Remarkable green fluorescence mainly in formulations coated with chitosan in the cytoplasm, higher chitosan content in FA-NP-12 showed some aggregates on the cell surface.

of chitosan properties was observed. The internalization of these self-assembled nanoplexes might thus be reduced by the preferential interaction between chitosan and the cell membrane.

3.6. Impact of surface charge on the uptake efficiency

A quantitative parameter for comparison of different formulations is the uptake efficiency. The number of transfected cells relative to the total number of cells was used as a measure of the transfection efficiency in different areas (~10 areas) of each sample.

While no uptake of fluorescent PLGA NPs was observed, around 50% of the cells were transfected with FA-NP-3, indicating the essential role of surface modification of NP with chitosan in improving the intracellular uptake of the particles, Fig. 7. However, the efficiency decreased gradually with higher amounts of chitosan to be <10% in case of FA-NP-12. Interestingly, the uptake efficiency of the different OMR/NP nanoplexes in A549 cells followed the same tendency as their corresponding plain FA-NPs; maximum uptake was recorded for NP-3 (~75%), followed by NP-6 and NP-9 (30–40%), and then NP-0 and NP-12 (<10%), Fig. 7.

In case of Calu-3 cells, the uptake efficiency of all NPs was <20% irrespective of the chitosan content.

From Fig. 7, the formulation giving maximum uptake efficiency was NP-3 with a positive charge of ~40 mV. One can thus assume that this magnitude of charge is the optimum for cellular uptake in A549 cells. In order to investigate this assumption, uptake studies in A549 cells were carried out using nanoplexes of FAM-OMR with NP-6, NP-9, and NP-12 in the OMR:NP weight ratio 1:15. At this ratio the overall ζ-potential was measured to be approximately comparable to that of OMR/NP-3 nanoplexes (ratio 1:50). CLSM images provided in Supplementary materials (Fig. S2) revealed a considerable increase in uptake in case of OMR/NP-6 and OMR/NP-9 nanoplexes, which was not observed in OMR/NP-12 nanoplexes.

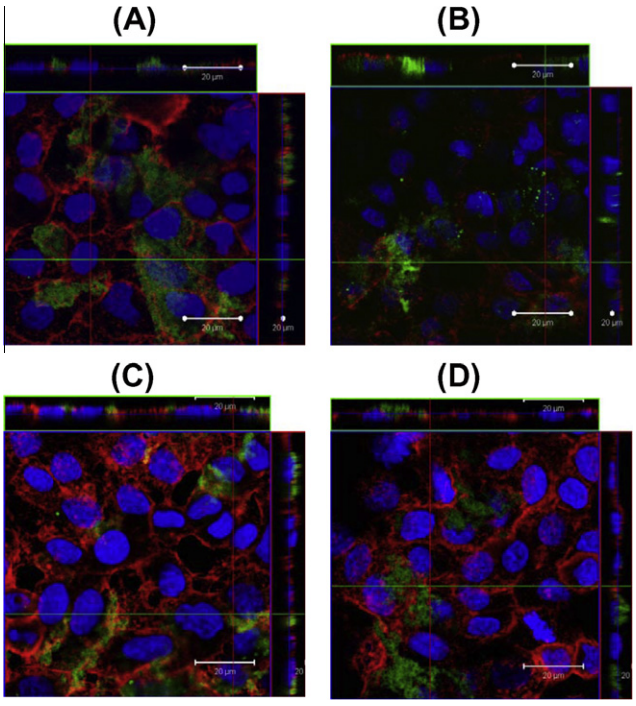

Fig. 6. CLSM images showing the uptake of self-assembled FAM-OMR nanoplexes with different types of chitosan in A549 cells: (A) CL113, (B) CL213, (C) CG113, (D) CG213. Green fluorescence: FAM-OMR, red fluorescence: cell membrane counterstained with RRCA and blue fluorescence: nuclei stained with DAPI. CLSM images 24 h after incubation show noticeable association with cell membrane and poor internalization.

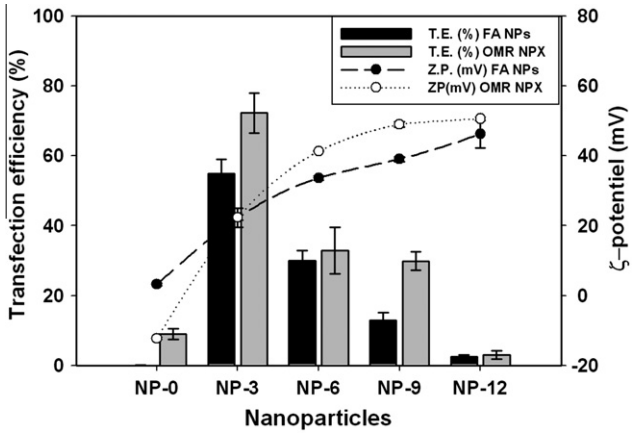

Fig. 7. Role of surface charge in enhancing the intracellular uptake: uptake efficiency and ζ-potential of different FA-NPs and OMR/FA-NPx as a function of chitosan concentration. Increasing chitosan gradually augment the ζ-potential of both nanoparticles (black circles) and nanoplexes (white circles). However, maximum uptake efficiency was recorded with NP-3 (black bar) and their corresponding nanoplexes with OMR (grey bars).

However, none of these nanoplexes reached the uptake efficiency of OMR/NP-3 (1:50), indicating that the positive charge cannot be considered the only parameter controlling the cellular uptake.

3.7. Nebulization of nanoparticles and uptake on air-interface cultures

Nanoparticles and nanoplexes sprayed with the hydraulic microsprayer, Penn Century®, retained their colloidal stability in terms of size (Fig. 8A), charge (Fig. 8B), and morphology as shown in the AFM images (Fig. 8C). In addition, the effect of the nebulization process on the membrane integrity and the cell viability was verified by means of LDH and MTT assays, (Fig. 8D and E, respectively) indicating that no cell damage by nebulization or direct particle deposition was observed. CLSM images, Fig. 8F, reveal the significantly higher amount of FAM-OMR internalized when applied as nanoplexes compared to the naked oligonucleotides and control cells. Further, the *xz*-sections showed the localization of nanoplexes in the cytoplasm as point-shaped spots, while naked oligonucleotides failed to be internalized and remain attached to the cell membrane.

3.8. TRAP assay

Improvement of cellular uptake should be accompanied with improved biological activity, which in our case is the inhibition of telomerase and in turn inhibition of cell proliferation.

Fig. 9 represents the telomerase activity in A549 cells treated with plain nanoparticles, nanoplexes of the antisense oligonucleotide with the nanoparticles (OMR-NPx), and nanoplexes of the mismatch with the nanoparticles (Mis-NPx). Plain nanoparticles with increasing chitosan content showed no remarkable reduction in telomerase activity (*Two-way ANOVA*, $p < 0.05$). Similarly, OMR alone as well as nanoplexes with PLGA nanoparticles without chitosan had no influence on telomerase activity, which might be attributed to the weak cellular uptake. Interestingly, OMR nanoplexes with chitosan-coated PLGA nanoparticles inhibited ~50% of telomerase activity in A549 cells relative to control 72 h after treatment (*Two-way ANOVA*, $p < 0.05$). The effect was less notable in case of OMR-NP-12, containing the highest chitosan content. To ensure the specificity of the response (telomerase inhibition), the experiment was simultaneously carried out using mismatch control (antisense oligonucleotide containing two mismatch bases relative to the template unit) instead of OMR. Results showed a reduction in telomerase activity to (~70–90%) with some formulations, but in all cases the telomerase inhibition was less pronounced compared to OMR-NPx, Fig. 9.

4. Discussion

Our previous study revealed that chitosan-modified PLGA nanoparticles can be prepared in a tunable way allowing flexible charge modification [19]. Measurement of the colloidal characteristics of OMR nanoplexes gave evidence of the adsorption of OMR molecules on the nanoparticle surface in a saturable way till charge reversal occur at equal OMR:NP weight ratios. The amount to be delivered is, hence, adjustable up to a maximum value.

The impact of the colloidal characteristics namely ζ-potential on cell binding, uptake, and telomerase activity was studied. The use of fluorescently labeled PLGA polymer was favorable over the encapsulation of a certain fluorescent dye in the nanoparticles. Fixing fluoresceinamine to the polymer by a covalent linkage was expected to guarantee stable fluorescent nanoparticles and minimize leakage of the fluorescent dye being in contact with the cell membrane along the uptake studies. Detailed investigations concerning the fluorescently labeled PLGA nanoparticles were previously fully described [24].

The presence of PLGA particles slightly improved uptake of FAM-OMR despite the weak fluorescence observed. The potential of PLGA nanoparticles as gene carrier following their uptake through an energy-dependent endocytotic process was previously reported [14,29]. The surface modification of PLGA nanoparticles with chitosan did not only improve the binding potential with OMR but also greatly enhanced the uptake of nanoplexes as revealed by the significant increase in uptake efficiency from <10%

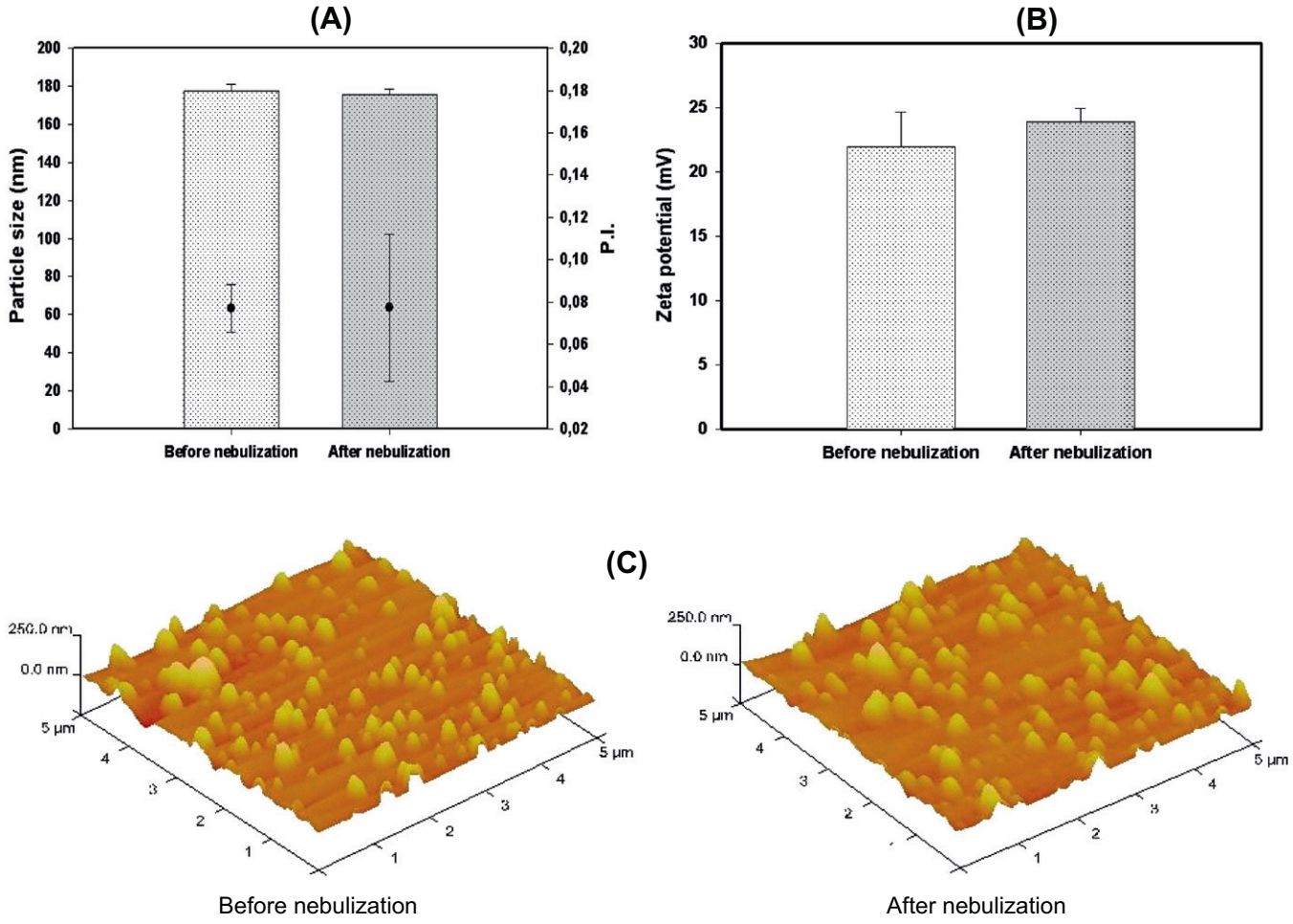

Fig. 8. Characterization of nanoparticles NP-3 before and after nebulization with the hydraulic microsprayer Penn Century: (A) particle size (bars) and PI (circles), (B) ζ-potential, (C) AFM images: Nebulized particles retained their colloidal characters and did not aggregate. (D) MTT assay, (F) LDH assay of air-interface cultured A549 cells after 6 h incubation with nebulized nanoparticles, (E) CLSM images showing significant uptake of nebulized FAM-OMR nanoplexes (green spots) on air-interface cultured A549 cells compared to FAM-OMR alone and control cells. Z stacks show intact cell membranes (red fluorescence) and green nanoplexes mainly in the cytoplasm.

to ~70% for OMR/NP-0 and OMR/NP-3 nanoplexes, respectively. Epithelial cells usually exhibit net negative surface charge due to the presence of negatively charged extracellular plasma membrane protein moieties [30]. This may account in part for the prolonged contact time and higher translocation rates of positively charged nanoparticles, NP-3, as compared with negatively charged particles, NP-0, in our study. This behavior was expected as the relevance of the surface charge of different types of particles such as polystyrene nanoparticles on their cellular uptake was previously studied [31–34]. In all these cases, a superior uptake of positively charged nanoparticles over negatively charged ones was demonstrated. Nevertheless, these data were not available for biodegradable chitosan-modified PLGA nanoparticles.

Investigating the influence of chitosan content on the cellular uptake, a linear relationship might have been expected. In contrast, an optimum chitosan concentration was found to be required for maximum uptake and transfection efficiency in A549 cells. Interestingly, the uptake behavior of OMR nanoplexes prepared with different NP formulations was in accordance with the uptake of fluorescently labeled plain nanoparticles. Further increase in chitosan content might negatively affect the uptake either due to preferential adsorption to the cellular membrane and due to increased agglomeration of the nanoparticles as shown in the confocal images, Figs. 4–6. Microscopical examination of the cell monolayer after incubation with different nanoparticle formulations showed that chitosan-coated nanoparticles remained attached to the cell surface even after several washing steps with PBS (refer to Fig. S3 in supplementary materials). This adhesion was more pronounced in case of nanoparticles with higher chitosan content, NP-12.

Indeed, we have previously studied the impact of culture medium on the colloidal stability of cationic nanoparticles. Our study demonstrated increased interaction of the positively charged NPs with serum proteins, divalent ions and the multicomponents in the culture medium forming agglomerates [35,36]. Agglomeration increased as a function of chitosan content. The bioadhesive properties of chitosan and agglomeration in culture medium might argue for the poor cellular uptake of NP-12. Similar studies on gold nanoparticles (14, 50, and 75 nm) showed that uptake into Hela cells reaches a plateau, mediated in part by non-specific adsorption of serum proteins to particles [37]. Besides, the finding that no steady increase in uptake of particles with higher surface charge suggests that cellular uptake should not only be attributed to surface charge but also to other surface properties such as hydrophilic/hydrophobic properties [33].

With regard to Calu-3 cells, the weak intracellular uptake observed in CLSM images supports the negligible increase in fluorescence detected by flow cytometry. Calu-3 cells are characterized by slow rate of division and growth compared to A549 cells; this might explain the relative weak uptake efficiency of the former.

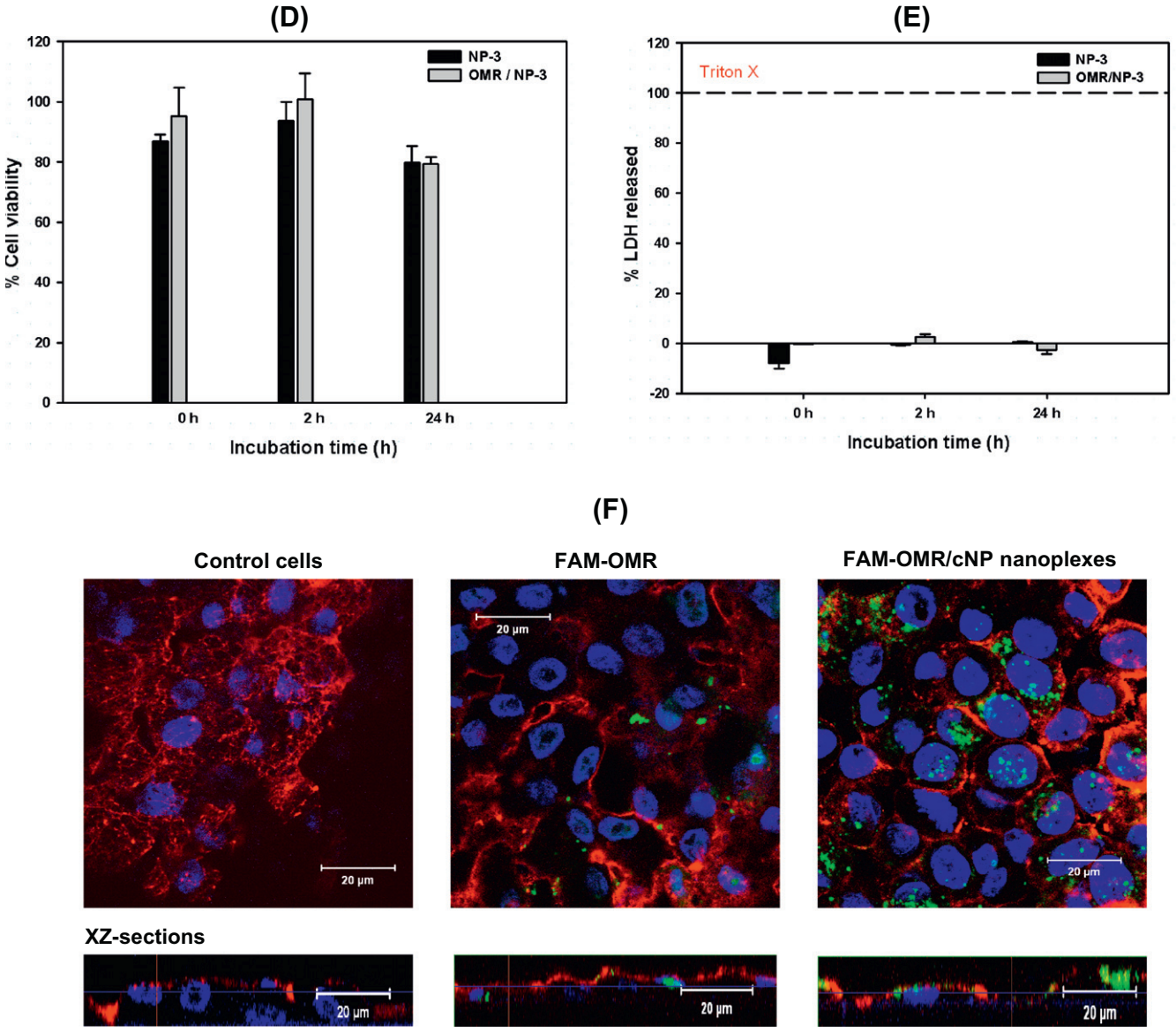

Fig. 8 (*continued*)

A higher level of transfection might be obtained if Calu-3 cells were allowed to grow and divide for longer durations.

To address the need for chitosan-coated nanoparticles instead of simple chitosan solution to deliver OMR as was always the case in many previous studies [38–40], both systems were tested and compared. Despite the ability of chitosan polymer to easily create self-assembled complexes with the negatively charged oligonucleotides, a strong association with cellular membrane was found rather than internalization (unlike the nanoparticles). It could be speculated that polymer conformation and flexibility have an impact. Self-assembled nanoplexes are known to acquire different shapes (circular, rods, ellipsoid, etc.); these complexes should be flexible enough to form agglomerating networks in presence of culture medium. These objects (shown in CLSM images) are retained on the cell surface. On the contrary, chitosan bound to nanoparticle surface is fixed rather than flexible and hence less prone to interaction. Chitosan-modified nanoparticles appear in CLSM images as well-defined spots not agglomerates. This underlines the superior efficacy of chitosan-modified PLGA NP over both plain PLGA NPs and chitosan solution as carrier for nucleotide-based drugs.

CLSM images revealed that the nanoparticles were localized mainly in the cytoplasm, while the nuclei were devoid of nanoparticles. Similar behavior was previously reported for polystyrene nanoparticles in rat alveolar epithelial cells [32] and gold nanoparticles in Hela cells [37] and alveolar macrophages [41]. However, mechanisms by which nanoparticles interact with the lung alveolar epithelium and their cellular fate once internalized are currently not well understood and require further investigation.

No clear impact of the chitosan properties on the uptake was observed. Similarly, Huang et al. showed that the uptake of chitosan molecules was independent of the molecular weight and degree of deacetylation [42].

To get a more realistic scenario for inhalation therapy, AIC was investigated instead of immersed systems. The hydraulic microsprayer, Penn Century®, had no negative influence on the colloidal characteristics of the nebulized nanoparticles or the integrity of the cell monolayer. This proves that the fluorescence observed in the cells resulted from a real uptake and not due to membrane perforation during spraying. Furthermore, nanoparticle deposition on the cell surface did not show harmful effects on the cell viability.

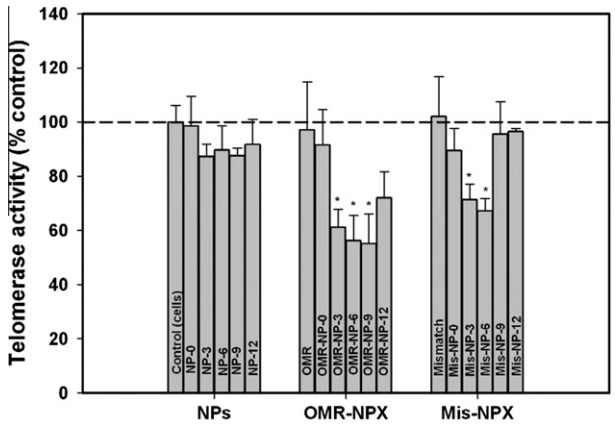

Fig. 9. TRAP assay: reduction of telomerase activity in A549 cells 72 h after incubation with plain nanoparticles, OMR nanoplexes and mismatch nanoplexes. Slight reduction in telomerase activity observed with cells incubated with chitosan-coated nanoparticles. Remarkable (~50%) reduction in case of OMR nanoplexes (*significant difference between OMR-NP-3, OMR-NP-6, OMR-NP-9 nanoplexes when compared to OMR alone, OMR-NP-0 and OMR-NP-12 nanoplexes, and also when compared to the corresponding plain nanoparticles in the first group, two-way ANOVA, $p < 0.05$). In addition, ~30% reduced activity observed when OMR was replaced by mismatch (*significant difference between Mis-NP-3, Mis-NP-6 nanoplexes when compared to Mis alone, Mis-NP-0, Mis-NP-9, and Mis-NP-12 nanoplexes, and also when compared to the corresponding plain nanoparticles in the first group, two-way ANOVA, $p < 0.05$).

Studying the uptake of nanoparticles and/or nanoplexes on AIC represents a real big step toward the *in vivo* expectations. The ability of our nanocarrier system to be internalized in a significant amount under these conditions while preserving the integrity of the cell monolayer enables to predict efficient pulmonary delivery in ongoing *ex vivo* studies using lung perfusion models and *in vivo* studies on experimental animals.

Several aspects can influence the nanoparticle uptake through AIC compared to conventional liquid cultures. Cells grown on air interface are known to be covered by a thin liquid film of pulmonary surfactants on their surface [43]. Once deposited within the lung lining via nebulization, nanoparticles are expected to interact with this surfactant film; this interaction will namely depend on the physicochemical properties of the nanoparticles and will definitely affect their uptake. It would be of interest to further study the interaction of our nanoplexes with lung surfactants as was done by many research groups on nanoparticles with different hydrophilic/hydrophobic characters [44,45].

Although the antisense oligonucleotide, OMR, is characterized as a potent telomerase inhibitor, its poor cellular uptake resulted in minor inhibition of telomerase activity. Loading of OMR on cationic nanoparticles significantly improved both the intracellular uptake and telomerase inhibition. However, the uptake efficiency and telomerase inhibition of different nanoplexes were not highly correlating (Fig. S4). Although NP-3 showed the maximum uptake, nanoplexes with NP-6 and NP-9 showed telomerase inhibition comparable to NP-3. This lead to the assumption that chitosan plays a distinct role in telomerase inhibition in a concentration-dependent way. The main difference between NP-3, NP-6, and NP-9 is the amount of chitosan on the nanoparticle surface. In other words, the higher chitosan concentration in NP-6 and NP-9 might have compensated their reduced uptake and hence showed comparable telomerase inhibition.

Despite the relatively weaker behavior of the mismatch, some mismatch-NPx showed a remarkable telomerase inhibition. These observations also contribute to our assumption (and ongoing research) that other parameters (e.g., chitosan on carrier system) most likely have an impact on telomerase inhibition.

Overall, efficient telomerase inhibition can drive cancer cells to apoptosis and limit tumor proliferation, while normal telomerase-free cells remain unaffected. This encouraged further studies on primary cell lines and tissue slices [46]. Yet it is not clear whether OMR affects hTR function while being complexed with the nanoparticles or had first to be released from the complex.

5. Conclusions

The study showed that chitosan-coated PLGA nanoparticles improved the loading, cellular uptake. As a consequence, pharmacological activity of the antisense oligonucleotide OMR could be observed. The particles were well tolerated by A549 and Calu-3 cells. Despite the essential role of chitosan, excessive chitosan content negatively affects the transfection efficiency. Self-assembled OMR nanoplexes with chitosan polymer alone are preferentially adsorbed to the cell membrane rather than being internalized. Thus, polymeric nanoparticles are superior to cationic polymers as carrier for antisense oligonucleotides. In conclusion, charge cannot be considered the principle factor behind improved transfection. Uptake studies carried out on air-interface cell cultures support the results on normal cultures showing enhanced uptake of nanoplexes compared to naked oligonucleotides representing an essential step toward the *in vivo* expectations.

Acknowledgements

This project is financially supported by Deutsche Krebshilfe e.V. (Project No.: 10-2035-Kl I) and the Robert Bosch Foundation (Stuttgart, Germany). The Egyptian Ministry of Education and the Deutscher Akademischer Austauschdienst (DAAD) are thanked for the scholarship.

Appendix A. Supplementary material

Supplementary data associated with this article can be found, in the online version, at doi:10.1016/j.ejpb.2011.11.019.

References

[1] A. Jemal, R. Siegel, J. Xu, E. Ward, Cancer statistics, CA: A Cancer Journal for Clinicians 60 (2010) 277–300.
[2] N. Debotton, M. Parnes, J. Kadouche, S. Benita, Overcoming the formulation obstacles towards targeted chemotherapy: in vitro and in vivo evaluation of cytotoxic drug loaded immunonanoparticles, Journal of Controlled Release 127 (2008) 219–230.
[3] H. Hwang, I.-S. Kim, I.C. Kwon, Y.-H. Kim, Tumor target ability and antitumor effect of docetaxel loaded hydrophobically modified glycol chitosan nanoparticles, Journal of Controlled Release 128 (2008) 23–31.
[4] G.R. Simon, M. Begum, G. Bepler, Setting the stage for tailored chemotherapy in the management of non-small cell lung cancer, Future Oncology 4 (2008) 51–59.
[5] T. Merdan, J. Kopecek, T. Kissel, Prospects for cationic polymers in gene and oligonucleotide therapy against cancer, Advanced Drug Delivery Reviews 54 (2002) 715–758.
[6] J. Wang, X. Tao, Y. Zhang, D. Wei, Y. Ren, Reversion of multidrug resistance by tumor targeted delivery of antisense oligodeoxynucleotides in hydroxypropyl-chitosan nanoparticles, Biomaterials 31 (2010) 4426–4433.
[7] G.B. Morin, The human telomere terminal transferase enzyme is a ribonucleoprotein that synthesizes TTAGGG repeats, Cell 59 (1989) 521–529.
[8] S. Taga, T. Osaki, A. Ohgami, H. Imoto, K. Yasumoto, Prognostic impact of telomerase activity in non-small cell lung cancers, Annals of Surgery 230 (1999) 715–720.
[9] B. Herbert, A.E. Pitts, S.I. Baker, S.E. Hamilton, W.E. Wright, J.W. Shay, D.R. Corey, Inhibition of human telomerase in immortal human cells leads to progressive telomere shortening and cell death, Proceedings of the National Academy of Sciences of the United States of America 96 (1999) 14276–14281.
[10] A.E. Pitts, D.R. Corey, Inhibition of human telomerase by 2′-O-methyl-RNA, Proceedings of the National Academy of Sciences of the United States of America 95 (1998) 11549–11554.
[11] M.C. Woodle, P.Y. Lu, Nanoparticles deliver RNAi therapy, Materials Today 8 (2005) 34–41.

[12] M. Wang, H.V. Adikane, J. Duhamel, P. Chen, Protection of oligodeoxynucleotides against nuclease degradation through association with self-assembling peptides, Biomaterials 29 (2008) 1099–1108.
[13] M. Morille, C. Passirani, A. Vonarbourg, A. Clavreul, J.-P. Benoit, Progress in developing cationic vectors for non-viral systemic gene therapy against cancer, Biomaterials 29 (2008) 3477–3496.
[14] N. Csaba, A. Sanchez, M.J. Alonso, PLGA: poloxamer and PLGA: poloxamine blend nanostructures as carriers for nasal gene delivery, Journal of Controlled Release 113 (2006) 164–172.
[15] S. Azarmi, W.H. Roa, R. Löbenberg, Targeted delivery of nanoparticles for the treatment of lung diseases, Advanced Drug Delivery Reviews 60 (2008) 863–875.
[16] L. Brannon-Peppas, J.O. Blanchette, Nanoparticle and targeted systems for cancer therapy, Advanced Drug Delivery Reviews Intelligent Therapeutics: Biomimetic Systems and Nanotechnology in Drug Delivery 56 (2004) 1649–1659.
[17] M. Shakweh, M. Besnard, V. Nicolas, E. Fattal, Poly (lactide-co-glycolide) particles of different physicochemical properties and their uptake by peyer's patches in mice, European Journal of Pharmaceutics and Biopharmaceutics 61 (2005) 1–13.
[18] U. Westedt, M. Kalinowski, M. Wittmar, T. Merdan, F. Unger, J. Fuchs, S. Schaller, U. Bakowsky, T. Kissel, Poly(vinyl alcohol)-graft-poly(lactide-co-glycolide) nanoparticles for local delivery of paclitaxel for restenosis treatment, Journal of Controlled Release 119 (2007) 41–51.
[19] N. Nafee, S. Taetz, M. Schneider, U.F. Schaefer, C.M. Lehr, Chitosan-coated PLGA nanoparticles for DNA/RNA delivery: effect of the formulation parameters on complexation and transfection of antisense oligonucleotides, Nanomedicine: Nanotechnology, Biology, and Medicine 3 (2007) 173–183.
[20] J.M. Dang, K.W. Leong, Natural polymers for gene delivery and tissue engineering, Advanced Drug Delivery Reviews Gene Delivery for Tissue Engineering 58 (2006) 487–499.
[21] V. Dodane, M. Amin Khan, J.R. Merwin, Effect of chitosan on epithelial permeability and structure, International Journal of Pharmaceutics 182 (1999) 21–32.
[22] H. Lin, H. Li, H.-J. Cho, S. Bian, H.-J. Roh, M.-K. Lee, J.S. Kim, S.-J. Chung, C.-K. Shim, D.-D. Kim, Air-liquid interface (ALI) culture of human bronchial epithelial cell monolayers as an in vitro model for airway drug transport studies, Journal of Pharmaceutical Sciences 96 (2007) 341–350.
[23] E. Horisawa, K. Kubota, I. Tuboi, K. Sato, H. Yamamoto, H. Takeuchi, Y. Kawashima, Size-dependency of DL-lactide/glycolide copolymer particulates for intra-articular delivery system on phagocytosis in rat synovium, Pharmaceutical Research 19 (2002) 132–139.
[24] B. Weiss, U.F. Schaefer, J. Zapp, A. Lamprecht, A. Stallmach, C.-M. Lehr, Nanoparticles made of fluorescently-labelled poly(L-lactide-co-glycolide): preparation, stability and biocompatibility, Journal of Nanoscience and Nanotechnology 6 (2006) 3048–3056.
[25] D.P. Joshi, Y.L. Lan-Chun-Fung, J.G. Pritchard, Determination of poly(vinyl alcohol) via its complex with boric acid and iodine, Analytica Chimica Acta 104 (1979) 153–160.
[26] R.A. Muzzarelli, Colorimetric determination of chitosan, Analytical Biochemistry 260 (1998) 255–257.
[27] B. Herbert, A. Hochreiter, W. Wright, J. Shay, Non-radioactive detection of telomerase activity using the telomeric repeat amplification protocol, Nature Protocols 1 (2006) 1583–1590.
[28] M. Khvedelidze, T. Mdzinarashvili, T. Partskhaladze, N. Nafee, U. Schaefer, C.-M. Lehr, M. Schneider, Calorimetric and spectrophotometric investigation of PLGA nanoparticles and their complex with DNA, Journal of Thermal Analysis and Calorimetry 99 (2010) 337–348.
[29] S. Prabha, W.-Z. Zhou, J. Panyam, V. Labhasetwar, Size-dependency of nanoparticle-mediated gene transfection: studies with fractionated nanoparticles, International Journal of Pharmaceutics 244 (2002) 105–115.
[30] Y. Rojanasakul, L. Wang, M. Bhat, D. Glover, C. Malanga, J. Ma, The transport barrier of epithelia: a comparative study on membrane permeability and charge selectivity in the rabbit, Pharmaceutical Research 9 (1992) 1029–1034.
[31] M.R. Lorenz, V. Holzapfel, A. Musyanovych, K. Nothelfer, P. Walther, H. Frank, K. Landfester, H. Schrezenmeier, V. Mailänder, Uptake of functionalized, fluorescent-labeled polymeric particles in different cell lines and stem cells, Biomaterials 27 (2006) 2820–2828.
[32] N.R. Yacobi, L. DeMaio, J. Xie, S.F. Hamm-Alvarez, Z. Borok, K.-J. Kim, E.D. Crandall, Polystyrene nanoparticle trafficking across alveolar epithelium, Nanomedicine: Nanotechnology, Biology and Medicine 4 (2008) 139–145.
[33] A. des Rieux, E.G.E. Ragnarsson, E. Gullberg, V. Préat, Y.-J. Schneider, P. Artursson, Transport of nanoparticles across an in vitro model of the human intestinal follicle associated epithelium, European Journal of Pharmaceutical Sciences 25 (2005) 455–465.
[34] M. Geiser, B. Rothen-Rutishauser, N. Kapp, S. Schürch, W. Kreyling, H. Schulz, M. Semmler, V. Im Hof, J. Heyder, P. Gehr, Ultrafine particles cross cellular membranes by nonphagocytic mechanisms in lungs and in cultured cells, Environmental Health Perspectives 113 (2005) 1555–1560.
[35] N. Nafee, M. Schneider, U.F. Schaefer, C.-M. Lehr, Relevance of the colloidal stability of chitosan/PLGA nanoparticles on their cytotoxicity profile, International Journal of Pharmaceutics 381 (2009) 130–139.
[36] C. Schulze, A. Kroll, C.-M. Lehr, U.F. Schaefer, K. Becker, J. Schnekenburger, C. Schulze Isfort, R. Landsiedel, W. Wohlleben, Not ready to use – overcoming pitfalls when dispersing nanoparticles in physiological media, Nanotoxicology 2 (2008) 51–61.
[37] B.D. Chithrani, A.A. Ghazani, W.C.W. Chan, Determining the size and shape dependence of gold nanoparticle uptake into mammalian cells, Nano Letters 6 (2006) 662–668.
[38] M.M. Issa, M. Koping-Hoggard, P. Artursson, Chitosan and the mucosal delivery of biotechnology drugs, Drug Discovery Today: Technologies 2 (2005) 1–6.
[39] M. Thanou, B.I. Florea, M. Geldof, H.E. Junginger, G. Borchard, Quaternized chitosan oligomers as novel gene delivery vectors in epithelial cell lines, Biomaterials 23 (2002) 153–159.
[40] S. Mansouri, P. Lavigne, K. Corsi, M. Benderdour, E. Beaumont, J.C. Fernandes, Chitosan–DNA nanoparticles as non-viral vectors in gene therapy: strategies to improve transfection efficacy, European Journal of Pharmaceutics and Biopharmaceutics 57 (2004) 1–8.
[41] S. Takenaka, E. Karg, W.G. Kreyling, B. Lentner, W. Mueller, M. Behnke-Semmler, L. Jennen, A. Walch, B. Michalke, P. Schramel, J. Heyder, H. Schulz, Distribution pattern of inhaled ultrafine gold particles in the rat lung, Inhalation Toxicology 18 (2006) 733–740.
[42] M. Huang, E. Khor, L.-Y. Lim, Uptake and cytotoxicity of chitosan molecules and nanoparticles: effects of molecular weight and degree of deacetylation, Pharmaceutical Research 21 (2004) 344–353.
[43] A. Meyboom, D. Maretzki, P.A. Stevens, K.P. Hofmann, Interaction of pulmonary surfactant protein A with phospholipid liposomes: a kinetic study on head group and fatty acid specificity, Biochimica et Biophysica Acta (BBA) – Molecular and Cell Biology of Lipids 1441 (1999) 23–35.
[44] D. Stuart, R. Löbenberg, T. Ku, S. Azarmi, L. Ely, W. Roa, E.J. Prenner, Biophysical investigation of nanoparticle interactions with lung surfactant model systems, Journal of Biomedical Nanotechnology 2 (2006) 245–252.
[45] L. Mu, P.H. Seow, Application of TPGS in polymeric nanoparticulate drug delivery system, Colloids and Surfaces B: Biointerfaces 47 (2006) 90–97.
[46] M. Dong, C. Philippi, B. Loretz, N. Nafee, U.F. Schaefer, G. Friedel, S. Ammon-Treiber, E.-U. Griese, C.-M. Lehr, U. Klotz, T.E. Mürdter, Tissue slice model of human lung cancer to investigate telomerase inhibition by nanoparticle delivery of antisense 2′-O-methyl-RNA, International Journal of Pharmaceutics 419 (2011) 33–42.